Far infrared synchrotron near-field nano-imaging and -spectroscopy

Omar Khatib,[1,2] Hans A. Bechtel*,[2] Michael C. Martin,[2] Markus B. Raschke*,[1] and G. Lawrence Carr*[3]

[1]*Department of Physics, Department of Chemistry, and JILA, University of Colorado, Boulder, CO 80309, USA*

[2]*Advanced Light Source Division, Lawrence Berkeley National Laboratory, Berkeley, CA 94720, USA*

[3]*National Synchrotron Light Source II, Brookhaven National Laboratory, Upton, NY 11973, USA**

(Dated: January 17, 2018)

*Email: habechtel@lbl.gov; markus.raschke@colorado.edu; carr@bnl.gov.

Scattering scanning near-field optical microscopy (*s*-SNOM) has emerged as a powerful imaging and spectroscopic tool for investigating nanoscale heterogeneities in biology, quantum matter, and electronic and photonic devices. However, many materials are defined by a wide range of fundamental molecular and quantum states at far-infrared (FIR) resonant frequencies currently not accessible by *s*-SNOM. Here we show ultrabroadband FIR *s*-SNOM nano-imaging and spectroscopy by combining synchrotron infrared radiation with a novel fast and low-noise copper-doped germanium (Ge:Cu)photoconductive detector. This approach of FIR synchrotron infrared nano-spectroscopy (SINS) extends the wavelength range of *s*-SNOM to 31μm (320 cm^{-1}, 9.7 THz), exceeding conventional limits by an octave to lower energies. We demonstrate this new nano-spectroscopic window by measuring elementary excitations of exemplary functional materials, including surface phonon polariton waves and optical phonons in oxides and layered ultrathin van der Waals materials, skeletal and conformational vibrations in molecular systems, and the highly tunable plasmonic response of graphene.

Near-field nanoscopy attracts increasing scientific attention, specifically in the implementation of infrared scattering type scanning near-field optical microscopy (IR *s*-SNOM) [1–4]. It provides for nano-imaging and -spectroscopy down to few nanometer length scales, gaining insight into molecular orientation [5] and coupling [6], catalytic activity [7], heterogeneity in electron and lattice dynamics [8, 9], and plasmonic and polaritonic effects in quantum matter [10–13] with recent extension to the low temperature [9, 14] and ultrafast regimes [15–18]. Despite these significant developments, *s*-SNOM has largely been limited to a narrow range of the electromagnetic spectrum of the near- to mid-IR at high frequencies, and the RF [19] and low THz [20] regime at low frequencies.

However, the far-infrared (FIR) spectral range (10 - 700 cm^{-1}, 14 - 1000 μm, 0.3 - 20 THz, 3 - 190K) has yet remained largely unexplored in *s*-SNOM, despite the significance of its low-energy molecular and quantum state resonances that define material functions from condensed matter physics to biology and medicine. Many fundamental excitations and collective modes in solids have characteristic energies in the FIR, including the free carrier Drude response, crystal lattice vibrations, charge density waves, superconducting energy gaps, magnetic excitations, surface plasmon and phonon polaritons, and others (Figure 1a)

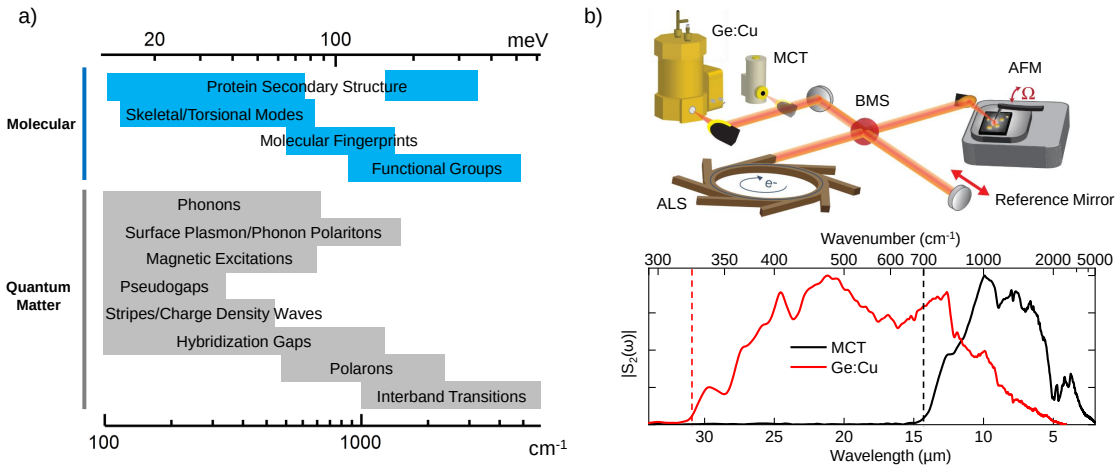

FIG. 1: a) Infrared energy scales and associated phenomena in molecular and quantum matter; b) *Top*: ultrabroadband SINS experimental configuration with extension to far-infrared frequencies; *bottom*: SINS reference spectrum using MCT (black curve) and Ge:Cu (red curve) detectors, demonstrating extended near-field spectroscopic performance at frequencies down to 320 cm^{-1}.

[21]. Similarly, in soft and biological molecular materials, the FIR provides spectral access to structurally specific ('fingerprint') vibrations and conformations via skeletal, torsional, and deformation modes, that allow for direct probing of, e.g., secondary structure in proteins [22].

The extension of *s*-SNOM into the FIR range has largely been hampered by the lack of both suitable light sources and detectors. On the high frequency side, IR *s*-SNOM is performed with different femtosecond laser based supercontinuum and parametric generation sources for broadband or broadly tunable mid-IR radiation, yet limited by suitable nonlinear optical crystals for frequency conversation to wavelengths < 18 μm [23]. At low frequencies, THz *s*-SNOM nano-imaging is performed with continuous wave THz sources, such as gas lasers and QCLs at a limited number of fixed frequencies [20, 24], or with broadband THz light generated from photoconductive antennas, limited to < 3 THz [25–27] and low power output.

To date far-IR *s*-SNOM has only routinely been achieved using a free electron laser (FEL) [28] that provides the necessary high intensity quasi-cw radiation as needed for *s*-SNOM spectroscopy. Although in principle continuously tunable from 1.5 - 75 THz (50 - 2500 cm^{-1}, 4 - 200 μm), nano-spectroscopy would be difficult, time consuming, and has

not yet been demonstrated. In contrary and most desirable for nano-spectroscopic imaging would be a broadband FIR light source with simultaneously high bandwidth and spectral irradiance across the full 10 - 30 THz (330 - 1000 cm^{-1}, 10 - 30 μm) spectral range. Not only does the enabled signal multiplexing and self-referencing eliminate multiple noise sources, but it also allows for the simultaneous probing of multiple characteristic material resonances, as desirable in monitoring kinetics of phase transitions or chemical transformations on the nanoscale.

In addition to limitations in the availability of suitable light sources is a lack of far-infrared detectors with the necessary speed and sensitivity for FIR *s*-SNOM. Mid-IR detectors based on small bandgap semiconductor alloys, such as $Hg_{1-x}Cd_xTe$ (MCT), have a long-wavelength cutoff typically at 600 cm^{-1}, with extension to lower frequency at the expense of drastically reduced sensitivity and challenged by material limitations. On the other hand, conventional FIR detectors such as pyroelectric deuterated triglycine sulfate (DTGS) or liquid helium cooled Si bolometers only operate at $<$ few kHz frequencies and have too slow response times. Extrinsic impurity photoconductors based on doped Si or Ge offer fast intrinsic response times ($<$ 100 ns) and small bandgaps in the FIR, yet in their usual implementation are plagued by excess thermal background and electronic noise, rendering them unsuitable for *s*-SNOM (see Supplementary Information for extended discussion).

In this letter, we demonstrate ultrabroadband near-field nano-spectroscopy covering the qualitatively new regime of far-IR *s*-SNOM. We utilize synchrotron radiation, which provides a low-noise, broadband, and coherent light source with high spectral irradiance spanning from THz to the extreme UV region [29]. To detect the tip-scattered near-field FIR signal we have developed a custom, MHz bandwidth Ge:Cu photoconductor with superior sensitivity for spectroscopic FIR *s*-SNOM nano-imaging. With this approach we are able to extend the wavelength range of *s*-SNOM by one octave, overcoming conventional limits, down to 31μm (320 cm^{-1}).

To demonstrate the performance in this new spectral regime, we probe previously inaccessible types of excitations with far-IR *s*-SNOM. This includes low energy phonons in anisotropic bulk crystalline media, as well as layered van der Waals systems, of interest for potential nano-photonics applications as natural hyperbolic materials. Skeletal deformations and torsional modes in organic semiconductor films allow for the simultaneous nano-probing of several vibrational degrees of freedom in molecular materials, which heavily influence

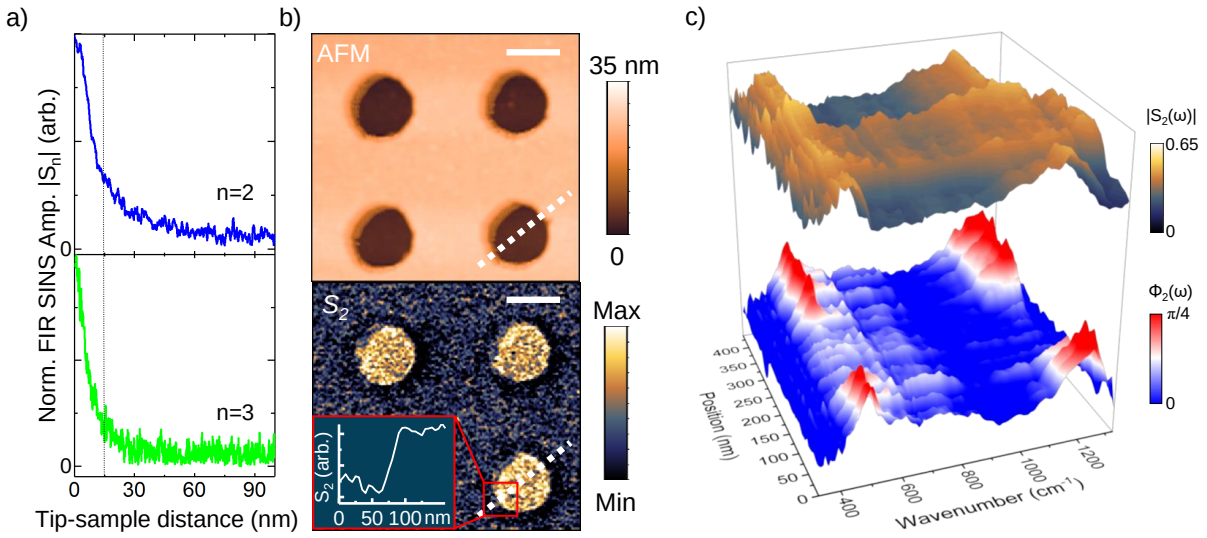

FIG. 2: FIR *s*-SNOM spatio-spectral characteristics. a) Tip-sample distance dependence in 2nd (blue trace) and 3rd (green trace) order demodulation of the tip tapping frequency (75-300 kHz). b) Far-IR nano-imaging of 25 nm-thick SiO_2 hole array, with AFM topography (top), and spectrally-integrated SINS amplitude signal S_2 (bottom), demonstrating near-field contrast between the patterned SiO_2 and underlying Si substrate with ~30 nm spatial resolution (inset). Scale bar is 200 nm. c) Spatio-spectral line scan (450 nm x 40 px) with trajectory indicated by dotted line in b), showing broadband SINS amplitude $S_2(\omega)$ (top) and phase $\Phi_2(\omega)$ (bottom) of asymmetric Si-O bend (460 cm^{-1}) and stretch (1200 cm^{-1}) phonon bands in SiO_2.

the low energy electronic and transport properties of functional devices. We access the THz plasmonic regime in graphene, including plasmon-phonon substrate interactions, and demonstrate a high degree of gate tunability. Lastly, we provide a platform to extend to yet longer wavelengths by combining with other extrinsic Ge detectors.

Figure 1b displays a schematic of the ultrabroadband *s*-SNOM nano-spectroscopy implementation, based on an atomic force microscope (AFM) using metal-coated tips, and interferometric detection as described previously [29]. IR synchrotron radiation is provided by the Advanced Light Source (ALS) at Lawrence Berkeley National Laboratory in two experimental configurations: Beamline 5.4, employing a specially modified AFM (Innova, Bruker) coupled to a commercial FTIR Spectrometer (Nicolet 6700, Thermo-Scientific), and Beamline 2.4 using a commercial nanoscope (neaSNOM, Neaspec GmbH), to measure the spectral near-field scattering amplitude and phase response $|S(\omega)|e^{i\Phi(\omega)}$. As a direct probe

of the sample dielectric function, broadband s-SNOM amplitude and phase typically exhibit simple dispersive and absorptive lineshapes, respectively, for weaker oscillators, and a more complicated hybrid response for strongly resonant and collective excitations [23, 30]. The customized LHe-cooled Ge:Cu detector for synchrotron infrared nano-spectroscopy (SINS) provides a broadband response (2 - 31 μm) and suitable sensitivity ($D^* > 10^{10} cm \cdot \sqrt{Hz}/W$). The low energy cutoff of Ge:Cu of 31 μm (320 cm^{-1}), limited by impurity band transitions from the Ge valence band edge, represents over a factor of two extension in wavelength compared to conventional MCTs (bottom panel in Fig. 1b). Complete details of the experimental setup, measurements, and Cu:Ge detector can be found in the Supplementary Information.

We first demonstrate the ultrahigh nanometer spatial resolution capability of FIR *s*-SNOM in SINS. Figure 2a,b shows the vertical and lateral field localization, respectively, of FIR synchrotron radiation by the AFM tip. *s*-SNOM approach curves (Fig. 2a) at 2nd and 3rd order tip demodulation (see Supplementary Information), demonstrate the few-nm confinement of the long wavelength tip-scattered light. Figure 2b shows a 1 μm^2 image of a patterned SiO_2/Si test sample with AFM topography (top) and spectrally-integrated FIR SINS amplitude $|S_2|$ (bottom), revealing strong dielectric contrast between SiO_2 and Si with $\sim$ 30 nm spatial resolution (Fig. 2b inset), corresponding to $\lambda/1100$.

Figure 2c shows a nano-spatiospectral line scan, reflecting the real and imaginary spectral dielectric response across a 200 nm hole in SiO_2, indicated by the white dotted line in Fig. 2b and normalized to a Au reference. The spectral features are the surface optical phonon polaritons of SiO_2, due to the asymmetric Si-O stretch vibration near 1200 cm^{-1} [30], and the previously inaccessible 460 cm^{-1} asymmetric Si-O bending mode [31]. This low energy mode is especially important for coupling to far-IR surface plasmons in ultrathin materials (see below), and highlights the ability of SINS for simultaneous probing of multiple spectrally separated material resonances with $<$ 30 nm spatial resolution.

We present additional FIR SINS spectra of representative classses of other material systems in Figure 3, which exhibit important low energy resonant features. Figure 3a first shows the FIR SINS spectra of SiO_2 with and without an ultrathin single sheet of graphene on top. The presence of monolayer graphene significantly modifies the local FIR response, with increased absorption as seen in the near-field phase due to the excitation and strong interaction between graphene plasmons and SiO_2 substrate phonons that we explore in more

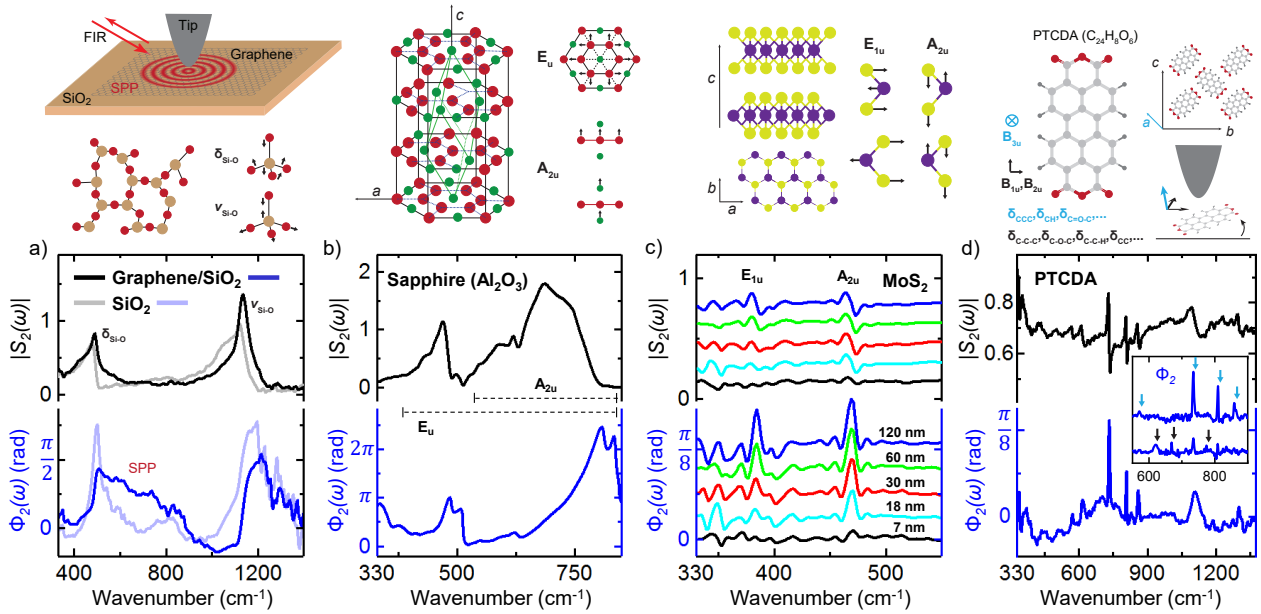

FIG. 3: FIR SINS amplitude $|S_2(\omega)|$ (top curves) and phase $\Phi_2(\omega)$ (bottom curves) spectra of selected material systems. a) SiO_2 with (dark traces) and without (light traces) a graphene overlayer, showing graphene plasmon-induced modification of the FIR near-field response. b) Low energy E_u and A_{2u} phonon bands for strongly resonant c-cut sapphire. d) Thickness-dependent E_{1u} in-plane and A_{2u} out-of-plane optical phonons of layered van der Waals material MoS_2. (d) Molecular semiconductor PTCDA, showing vibrational modes from skeletal deformations in the IR fingerprint range. Inset compares $\Phi_2(\omega)$ for two adjacent crystal grains with differing orientation, with the respective IR-active modes indicated by arrows. Cartoon schematics above data panels depict the resonant excitations probed by tip.

detail below. Strong light-matter interactions in the near-field for polar dielectrics and other crystalline materials can result in very large scattering amplitudes exceeding highly reflective non-resonant surfaces such as Au. Figure 3b shows the reststrahlen region of c-cut sapphire (Al_2O_3) for its E_u and A_2u optical phonon branches, covering the range where its hyperbolic response is due to an intrinsic optical anisotropy [32].

Using FIR SINS, we have the sensitivity to even probe weak excitations in layered and molecular materials. Figure 3c shows van der Waals material MoS_2, with its A_{2u} out-of-plane mode at 468 cm^{-1} and E_{1u} in-plane mode [33] at 384 cm^{-1} for a number of exfoliated flakes of different thicknesses. We are able to discern these phonon features for MoS_2 layers down to 7 nm in thickness, demonstrating a unique symmetry sensitivity, even in layered

systems with small interlayer coupling. FIR SINS can also be used as an orientational probe in molecular solids. Figure 3d shows a range of skeletal and deformation modes in the aromatic ring structure of organic semiconductor perylenetetracarboxylic dianhydride (PTCDA), including both in-plane (B_{1u}, B_{2u}) and out-of-plane (B_{3u}) bending vibrations (e.g. δ_{C-C-C}, $\delta_{C=O-C}$, etc.) [34], for a relatively uniform, thick film. The relative intensity of these modes can be used to map the spatial distribution at the single crystallite level [5], as seen by comparing two adjacent PTCDA grains within a few hundred nanometers in a more heterogeneous area of the sample (Fig. 3d inset).

Investigation of molecular and low-dimensional materials often necessitates controlled modification of external parameters. Graphene attracts much attention because of its inherently tunable IR and THz plasmonic response, though extremely sensitive to local interactions and coupling to the underlying substrate. Figure 4a demonstrates modulation of the far-IR SINS signal of a functional graphene/SiO_2 device subject to *in situ* electrostatic tuning of the back gate voltage V_{GS}. We observe a significant modification of the far-IR response with gate bias, with a strong enhancement of both $|S_2(\omega)|$ (top, red shaded curves) and $\Phi_2(\omega)$ (bottom, blue shaded curves) for negative voltages, and a nearly full suppression for high positive voltages above +50 V, approaching the intrinsic response of the underlying SiO_2 (black curve).

The voltage-dependent response of graphene additionally displays strong far-IR contrast in spectrally-integrated SINS nano-imaging (Fig. 4b), with a bright stripe within few hundred nm of the graphene/SiO_2 edge at low gate bias (middle panel), whereas at higher voltage the image contrast weakens and becomes more uniform with the adjacent SiO_2 substrate (bottom panel). Lastly, Fig. 4c reveals a rich spectral structure in $|S_2(\omega)|$ and $\Phi_2(\omega)$ confined to within 300 nm of the graphene/SiO_2 interface, yet at far-IR wavelengths down to 31 μm. The spectral response observed is the result of gate-tuning of the free carrier Drude response in graphene, superimposed with the excitation of surface plasmon polariton waves that are launched by the metallic probe tip, and propagate radially away and interfere with reflected waves from the graphene/SiO_2 edge, observed previously in monochromatic mid-IR *s*-SNOM nano-imaging [10, 11, 35]. The combined data in Fig. 4 thus demonstrate expansion into the FIR plasmon tuning range of graphene, opening a new regime in this and related 2D materials.

The material responses probed in this work demonstrate the capability of FIR SINS

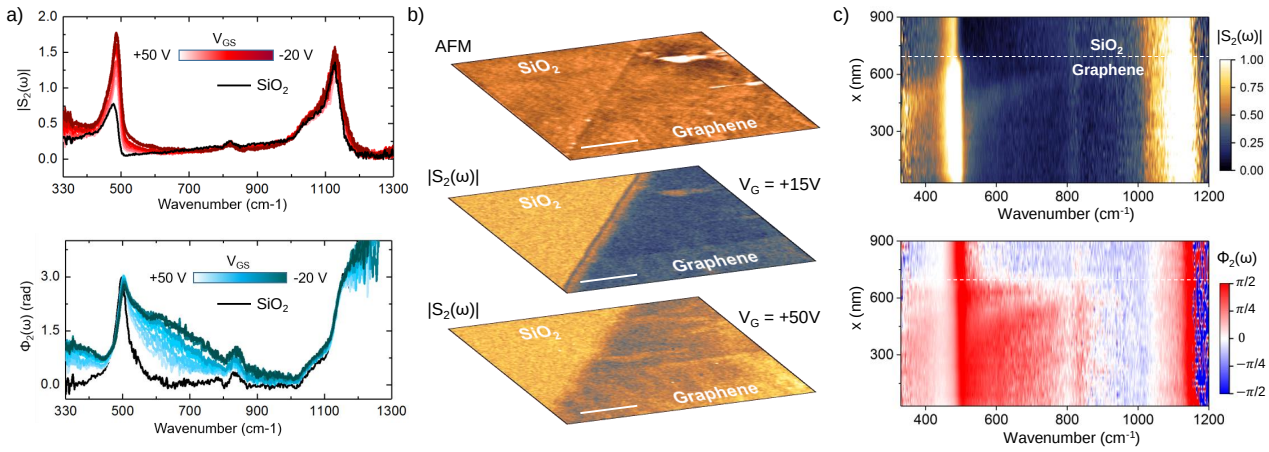

FIG. 4: Far-IR graphene plasmonics. a) Gate-tuning of SINS amplitude $|S_2(\omega)|$ (red shaded curves) and phase $\Phi_2(\omega)$ (blue shaded curves) for a functional graphene device on SiO_2 (black line), showing modulation of free carrier Drude response and plasmon absorption in graphene. b) SINS nano-imaging of graphene/SiO_2 interface for highly-doped (V_{GS} = +15 V, middle panel) and low-doped (V_{GS} = +50 V, bottom panel) graphene. c) SINS spatio-spectral line scan across doped-graphene/SiO_2 boundary, demonstrating nanometer broadband spectroscopic access to far-IR surface plasmon polariton (SPP) waves in graphene down to 320 cm^{-1}. The SPP dispersion as a function of energy can be observed directly near the graphene edge, where reflected surface waves constructively interfere with those launched from the AFM tip.

for new scientific investigations previously unavailable in s-SNOM. The low energy optical phonon regime in solids is critical to studies ranging from thermal transport and electron-phonon scattering in low dimensional materials [36] to mediating interactions in strongly correlated materials and superconductors [37]. The wide spectral coverage of FIR SINS allows for simultaneous nano-probing of free carriers in weakly metallic systems and other collective modes such as magnetic or charge density wave excitations [21]. Additionally, the high sensitivity to weak flexural and torsional modes in molecular materials (Fig. 3d) can be used to disentangle competing effects in for example organic semiconductors, where charge dynamics are dominated by a complex interplay of structural and vibrational nanoscale disorder, giving rise to localized excitations such as polarons [38].

The promise of tunable graphene plasmonics is already being exploited for the development of novel nano-photonics applications from visible to THz frequencies [39]. As an

atomically thin layer, there is great interest in coupling graphene plasmons to other vibrations in adjacent layers or substrates, given its high sensitivity to the immediate environment [40]. As seen in Fig. 4, with FIR SINS we observe a significant enhancement of the low energy SiO_2 phonon mode and direct absorption of graphene plasmons, suggesting a very strong plasmon-phonon coupling that is highly tunable with gating. This also opens up new opportunities for studying a wide range of corresponding modes in 2D and Dirac materials, including transition metal dichalcogenides, black phosphorous, and topological insulators, which typically host plasmons at FIR energies [13]. Further, large intrinsic anisotropies in these and other polar dielectric crystals can be explored for use as natural hyperbolic materials for unique nano-photonics applications in the FIR, without the need for artificial metamaterials with high losses [41], all with nanoscale spatial resolution.

Our approach can be further extended towards lower THz frequencies below 300 cm^{-1}, for example by choosing other Ge or Si impurity conductors such as Ge:Zn (2 - 40 μm) or Ge:Ga (30 - 100 μm). While conventional helium-cooled Si bolometers, which are typically used for far-IR measurements in the far-field, have the necessary sensitivity (NEP $<$ pW/$Hz^{0.5}$) and spectral bandwidth (10 - 1000 cm^{-1}), they are exceedingly slow in their standard configuration with detection speeds of $<$1 kHz. Superconducting hot electron bolometers offer another possibility for this spectral range, with sufficient speed and broadband coverage from 30 - 1000 cm^{-1}, but sensitivity often limited to $\sim$ 10 pW/$Hz^{0.5}$. Recent antenna-coupled Nb bolometers, however, have demonstrated and sub-ns response time and NEP of 20 fW/$Hz^{0.5}$ [42]. Alternative detection schemes such as non-synchronized electro-optic sampling, which directly measures the electric field, have also been shown to be compatible for continuous wave sources up to 40 THz [43]. Lastly, we believe detector electronics can be improved to further reduce electronic noise, ultimately achieving photon noise-limited detection (see Supplementary Information for extended discussion).

In conclusion, we have demonstrated a qualitatively new regime of IR *s*-SNOM nanoimaging and -spectroscopy through far-infrared SINS. Utilizing the spatial coherence, high spectral irradiance, and ultrabroadband properties of synchrotron IR radiation, combined with a custom low-noise fast modulating Ge:Cu photoconductor, we are able to provide nanospectroscopic capabilities to wavelengths down to to 31μm (320 cm^{-1}) with ultrahigh 30 nm spatial resolution. We demonstrate unique spatiospectral access to a range of resonant far-IR electronic and lattice excitations, including the low-energy free carrier response, surface

phonon polariton waves and optical phonons in oxides and ultrathin van der Waals materials, skeletal deformations and conformational vibrations in molecular systems, and the highly tunable FIR plasmonic regime of graphene. With continued detector development, it is possible to further extend the range of FIR SINS to ultimately bridge the energy gap with available THz *s*-SNOM sources, yet in a single nano-spectroscopy instrument. This work highlights the continued advantage of synchrotron radiation as an ultrabroadband coherent light source for near-field nano-spectroscopy, especially in the long wavelength regime where alternative low-noise, broadband, quasi-cw laser sources are not readily available.

I. ACKNOWLEDGEMENTS

M.B.R. acknowledges support from the NSF Science and Technology Center on Real-Time Functional Imaging under DMR-1548924 for development of FIR *s*-SNOM, and the US Department of Energy, Office of Basic Sciences, Division of Material Sciences and Engineering, under award no. DE-SC0008807 for the graphene device application. The Advanced Light Source is supported by the Director, Office of Science, Office of Basic Energy Sciences, of the U.S. Department of Energy under contract no. DE-AC02- 05CH11231. O.K. acknowledges support from the ALS Postdoctoral Fellowship program. The authors thank Sheng Wang and Feng Wang for providing a functional graphene device, and Sam Berweger for preparing exfoliated flakes of MoS_2.

---

[1] Zenhausern, F., Martin, Y., and Wickramasinghe, H. K. *Science* **269**(5227), 1083 August (1995).

[2] Knoll, B. and Keilmann, F. *Nature* **399**, 134 May (1999).

[3] Taubner, T., Hillenbrand, R., and Keilmann, F. *Journal of Microscopy* **210**(3), 311–314 June (2003).

[4] Atkin, J. M., Berweger, S., Jones, A. C., and Raschke, M. B. *Advances in Physics* **61**(6), 745–842 December (2012).

[5] Muller, E. A., Pollard, B., Bechtel, H. A., van Blerkom, P., and Raschke, M. B. *Sci Adv* **2**(10) October (2016).

[6] Pollard, B., Muller, E. A., Hinrichs, K., and Raschke, M. B. *Nature Communications* **5**, 3587 April (2014).

[7] Wu, C.-Y., Wolf, W. J., Levartovsky, Y., Bechtel, H. A., Martin, M. C., Toste, F. D., and Gross, E. *Nature* **541**(7638), 511–515 January (2017).

[8] Qazilbash, M. M., Brehm, M., Chae, B.-G., Ho, P.-C., Andreev, G. O., Kim, B.-J., Yun, S. J., Balatsky, A. V., Maple, M. B., Keilmann, F., Kim, H.-T., and Basov, D. N. *Science* **318**(5857), 1750 December (2007).

[9] McLeod, A. S., van Heumen, E., Ramirez, J. G., Wang, S., Saerbeck, T., Guenon, S., Goldflam, M., Anderegg, L., Kelly, P., Mueller, A., Liu, M. K., Schuller, I. K., and Basov, D. N. *Nat Phys* **13**(1), 80–86 January (2017).

[10] Fei, Z., Rodin, A. S., Andreev, G. O., Bao, W., McLeod, A. S., Wagner, M., Zhang, L. M., Zhao, Z., Thiemens, M., Dominguez, G., Fogler, M. M., Neto, A. H. C., Lau, C. N., Keilmann, F., and Basov, D. N. *Nature* **487**(7405), 82–85 July (2012).

[11] Chen, J., Badioli, M., Alonso-Gonzalez, P., Thongrattanasiri, S., Huth, F., Osmond, J., Spasenovic, M., Centeno, A., Pesquera, A., Godignon, P., Zurutuza Elorza, A., Camara, N., de Abajo, F. J. G., Hillenbrand, R., and Koppens, F. H. L. *Nature* **487**(7405), 77–81 July (2012).

[12] Dai, S., Fei, Z., Ma, Q., Rodin, A. S., Wagner, M., McLeod, A. S., Liu, M. K., Gannett, W., Regan, W., Watanabe, K., Taniguchi, T., Thiemens, M., Dominguez, G., Neto, A. H. C., Zettl, A., Keilmann, F., Jarillo-Herrero, P., Fogler, M. M., and Basov, D. N. *Science* **343**(6175), 1125 March (2014).

[13] Basov, D. N., Fogler, M. M., and Garca de Abajo, F. J. *Science* **354**(6309) October (2016).

[14] Yang, H. U., Hebestreit, E., Josberger, E. E., and Raschke, M. B. *Review of Scientific Instruments* **84**(2), 023701 February (2013).

[15] Wagner, M., McLeod, A. S., Maddox, S. J., Fei, Z., Liu, M., Averitt, R. D., Fogler, M. M., Bank, S. R., Keilmann, F., and Basov, D. N. *Nano Lett.* **14**(8), 4529–4534 August (2014).

[16] Eisele, M., Cocker, T. L., Huber, M. A., Plankl, M., Viti, L., Ercolani, D., Sorba, L., Vitiello, M. S., and Huber, R. *Nat Photon* **8**(11), 841–845 November (2014).

[17] Atkin, J. M., Sass, P. M., Teichen, P. E., Eaves, J. D., and Raschke, M. B. *J. Phys. Chem. Lett.* **6**(22), 4616–4621 November (2015).

[18] Dönges, S. A., Khatib, O., O'Callahan, B. T., Atkin, J. M., Park, J. H., Cobden, D., and

Raschke, M. B. *Nano Lett.* **16**(5), 3029–3035 May (2016).

[19] Lai, K., Ji, M. B., Leindecker, N., Kelly, M. A., and Shen, Z. X. *Review of Scientific Instruments* **78**(6), 063702 June (2007).

[20] Huber, A. J., Keilmann, F., Wittborn, J., Aizpurua, J., and Hillenbrand, R. *Nano Lett.* **8**(11), 3766–3770 November (2008).

[21] Liu, M., Sternbach, A. J., and Basov, D. N. *Reports on Progress in Physics* **80**(1), 014501 (2017).

[22] Falconer, R. J., Zakaria, H. A., Fan, Y. Y., Bradley, A. P., and Middelberg, A. P. J. *Appl Spectrosc* **64**(11), 1259–1264 November (2010).

[23] Huth, F., Govyadinov, A., Amarie, S., Nuansing, W., Keilmann, F., and Hillenbrand, R. *Nano Lett.* **12**(8), 3973–3978 August (2012).

[24] Degl'Innocenti, R., Wallis, R., Wei, B., Xiao, L., Kindness, S. J., Mitrofanov, O., Braeuninger-Weimer, P., Hofmann, S., Beere, H. E., and Ritchie, D. A. *ACS Photonics* August (2017).

[25] von Ribbeck, H.-G., Brehm, M., van der Weide, D. W., Winnerl, S., Drachenko, O., Helm, M., and Keilmann, F. *Opt. Express* **16**(5), 3430–3438 March (2008).

[26] Moon, K., Do, Y., Lim, M., Lee, G., Kang, H., Park, K.-S., and Han, H. *Appl. Phys. Lett.* **101**(1), 011109 July (2012).

[27] Kurihara, T., Yamaguchi, K., Watanabe, H., Nakajima, M., and Suemoto, T. *Appl. Phys. Lett.* **103**(15), 151105 October (2013).

[28] Kuschewski, F., von Ribbeck, H.-G., Dring, J., Winnerl, S., Eng, L. M., and Kehr, S. C. *Appl. Phys. Lett.* **108**(11), 113102 March (2016).

[29] Bechtel, H. A., Muller, E. A., Olmon, R. L., Martin, M. C., and Raschke, M. B. *Proceedings of the National Academy of Sciences* **111**(20), 7191–7196 May (2014).

[30] Amarie, S. and Keilmann, F. *Phys. Rev. B* **83**(4), 045404 January (2011).

[31] Kitamura, R., Pilon, L., and Jonasz, M. *Appl. Opt.* **46**(33), 8118–8133 November (2007).

[32] Schubert, M., Tiwald, T. E., and Herzinger, C. M. *Phys. Rev. B* **61**(12), 8187–8201 March (2000).

[33] Zhang, X., Qiao, X.-F., Shi, W., Wu, J.-B., Jiang, D.-S., and Tan, P.-H. *Chem. Soc. Rev.* **44**(9), 2757–2785 (2015).

[34] Kobitski, A. Y., Scholz, R., and Zahn, D. R. T. *Journal of Molecular Structure: THEOCHEM* **625**(1), 39–46 May (2003).

[35] Gerber, J. A., Berweger, S., O'Callahan, B. T., and Raschke, M. B. *Phys. Rev. Lett.* **113**, 055502 Jul (2014).

[36] Subhash L. Shind, G. P. S., editor. *Length-Scale Dependent Phonon Interactions*. Springer, New York, NY, (2014).

[37] Basov, D. N., Averitt, R. D., van der Marel, D., Dressel, M., and Haule, K. *Rev. Mod. Phys.* **83**(2), 471–541 June (2011).

[38] Sakanoue, T. and Sirringhaus, H. *Nature Materials* **9**, 736 August (2010).

[39] Garca de Abajo, F. J. *ACS Photonics* **1**(3), 135–152 March (2014).

[40] Low, T. and Avouris, P. *ACS Nano* **8**(2), 1086–1101 February (2014).

[41] Narimanov, E. E. and Kildishev, A. V. *Nature Photonics* **9**, 214 March (2015).

[42] Santavicca, D. F., Annunziata, A. J., Reese, M. O., Frunzio, L., and Prober, D. E. *Superconductor Science and Technology* **20**(11), S398 (2007).

[43] Gaal, P., Raschke, M. B., Reimann, K., and Woerner, M. *Nature Photonics* **1**, 577 October (2007).